Spatially dependent flood probabilities to support the design of civil infrastructure systems

Phuong Dong Le[1,2], Michael Leonard[1], Seth Westra[1]

[1]*School of Civil, Environmental and Mining Engineering, University of Adelaide, Adelaide, South Australia, Australia*

[2]*Thuyloi University, Hanoi, Vietnam*

Email: lephuongdong_tb@tlu.edu.vn

Keywords: areal reduction factor, asymptotic independence, conditional probability, duration dependence, extreme rainfall, flood probability, inverted max-stable process, joint probability, spatially dependent Intensity-Duration-Frequency

Abstract

Conventional flood risk methods typically focus on estimation at a single location, which can be inadequate for civil infrastructure systems such as road or railway infrastructure. This is because rainfall extremes are spatially dependent, so that to understand overall system risk it is necessary to assess the interconnected elements of the system jointly. For example, when designing evacuation routes it is necessary to understand the risk of one part of the system failing given that another region is flooded or exceeds the level at which evacuation becomes necessary. Similarly, failure of any single part of a road section (e.g., a flooded river crossing) may lead to the wider system's failure (i.e. the entire road becomes inoperable). This study demonstrates a spatially dependent Intensity-Duration-Frequency framework that can be used to estimate flood risk across multiple catchments, accounting for dependence both in space and across different critical storm durations. The framework is demonstrated via a case study of a highway upgrade, comprising five river crossings. The results show substantial differences in conditional and unconditional design flow estimates, highlighting the importance of taking an integrated approach. There is also a reduction in the estimated failure probability of the overall system compared with the case where each river crossing is treated independently. The results demonstrate the potential uses of spatially dependent Intensity-Duration-Frequency methods and suggest the need for more conservative design estimates to take into account conditional risks.

1. Introduction

Methods for quantifying the flood risk of civil infrastructure systems such as road and rail networks require considerably more information compared to traditional methods that focus on flood risk at a point. For example, the design of evacuation routes requires the quantification of the risk that one part of the system will fail at the same time that another region is flooded or exceeds the level at which evacuation becomes necessary. Similarly, a railway route may become impassable if any of a number of bridges are submerged, such that the 'failure probability' of that route becomes some aggregation of the failure probabilities of each individual section. Successful estimation of flood risk in these systems therefore requires recognition both of the networked nature of the civil infrastructure system across a spatial domain, as well as the spatial and temporal structure of flood-producing mechanisms (e.g. storms and extreme rainfall) that can lead to system failure (e.g., Leonard et al. (2014), Seneviratne et al. (2012), Zscheischler et al. (2018)).

One way to estimate such flood probabilities is to directly use information contained in historical streamflow data. For example, annual maximum streamflow at two locations might be assumed to follow a bivariate generalized extreme value distribution (Favre et al., 2004; Wang, 2001; Wang et al., 2009), which can then be used to estimate both conditional probabilities (e.g. the probability that one river is flooded given that the other river level exceeds a specified threshold) and joint probabilities (e.g. the probability that one or both rivers are flooded). Several frameworks have been demonstrated based directly on streamflow observations, including functional regression (Requena et al., 2018), multisite copulas (Renard and Lang, 2007), and spatial copulas (Durocher et al., 2016). However, in many instances continuous streamflow data are unavailable or insufficient at the locations of interest, or the catchment conditions have changed such that historical streamflow records as unrepresentative of likely future risk. For these situations, rainfall-based methods are often more appropriate.

There are two primary classes of rainfall-based methods to estimate flood probability. The first uses continuous rainfall data (either historical or generated) to compute continuous streamflow data using a rainfall-runoff model (Boughton and Droop, 2003; Cameron et al., 1999; He et al., 2011; Hegnauer et al., 2014; Pathiraja et al., 2012), with flood risk then estimated based on the simulated streamflow time

series. This method is computationally intensive and given the challenge of reproducing a wide variety of statistics across many scales, can have difficulties in modelling the dependence of extremes. Most spatial rainfall models operate at the daily timescale (Bárdossy and Pegram, 2009; Baxevani and Lennartsson, 2015; Bennett et al., 2016b; Hegnauer et al., 2014; Kleiber et al., 2012; Rasmussen, 2013), whereas many catchments respond at sub-daily timescales. This is likely to be because the capacity of space-time rainfall models to simulate the statistics of sub-daily rainfall remains a challenging research problem (Leonard et al., 2008), although one approach is to exploit the relative abundance of data at the daily scale, then apply a downscaling model to reach sub-daily scales (Gupta and Tarboton, 2016). Continuous simulation is receiving ongoing attention and increasing application, yet there remain limitations when applying these models in many practical contexts.

The second rainfall-based method proceeds by applying probability calculations on rainfall, to construct 'Intensity-Duration-Frequency' (IDF) curves, which are then translated to a runoff event of equivalent probability either via empirical models such as the rational method to estimate peak flow rate (Kuichling, 1889; Mulvaney, 1851), or via event-based rainfall-runoff models that are able to simulate the full flood hydrograph (Boyd et al., 1996; Chow et al., 1988; Laurenson and Mein, 1997). Regional frequency analysis is one type of method to estimate IDF values, where the precision of at-site estimates is improved by pooling data from sites in the surrounding region (Hosking and Wallis, 1997). These methods can be combined with spatial interpolation methods to estimate parameters for any ungauged location of interest (Carreau et al., 2013). To determine an effective mean depth of rainfall over a catchment with the same exceedance probability as at a gauge location, the pointwise estimate of extreme rainfall is multiplied by an areal reduction factor (ARF) (Ball et al., 2016). However, such methods do not account for information on the spatial dependence of extreme rainfall—whether for a single storm duration, or for the more complex case of different durations across a region (Bernard, 1932; Koutsoyiannis et al., 1998). The underlying independence assumption prevents these approaches from being applied to estimate conditional or joint flood risk at multiple points in a catchment or across several catchments, as would be required for a civil infrastructure system.

Although multivariate approaches can be tailored to estimate conditional and joint probabilities of extreme rainfall for specific situations (e.g., Kao and Govindaraju (2008), Wang et al. (2010), Zhang and Singh (2007)), the development of a unified methodology that integrates with existing IDF-based flood estimation approaches remains elusive. This is particularly challenging given that it is not only necessary to account for dependence of rainfall across space, but also to account for dependence across storm burst durations, as different parts of the system may be vulnerable to different critical duration storm events. To this end, max-stable process theory has been demonstrated to represent storm-level dependence (de Haan, 1984; Schlather, 2002) and used to calculate conditional probabilities for a spatial domain (Padoan et al., 2010). Copulas including the extremal-t copula (Demarta and McNeil, 2005), and the Husler-Reiss copula (Hüsler and Reiss, 1989) have also been used to model rainfall dependence.

This study applies a max-stable approach with an emphasis on practical flood estimation problems. To this end, any proposed approach needs to account for:

1. The spatial dependence of rainfall 'events' both for single durations, and also across multiple different durations. This was addressed by Le et al. (2018b), who linked a max-stable model with the duration-dependent model of Koutsoyiannis et al. (1998), to create a model that could be used to reflect dependencies between nearby catchments of different sizes.
2. The asymptotic properties of spatial dependence as the events become increasingly extreme, given the focus of many flood risk estimation methods on rare flood events. Recent evidence is emerging that rainfall has an asymptotically independent characteristic (Le et al., 2018a; Thibaud et al., 2013), which means that the level of the rainfall's dependence reduces with an increasing return period (Wadsworth and Tawn, 2012). The requirement of asymptotic independence indicates that inverted max-stable models are preferable over max-stable models.

This study adapts the methods developed by Le et al. (2018b) to inverted max-stable models to derive spatially-dependent IDF estimates and ARFs as the basis for transforming rainfall into flood flows. The approach is demonstrated on a highway system spanning 20 km with five separate river crossings.

The case study is designed to address two related questions: (i) "What flood flow needs to be used to design a bridge that will fail on average only once on average every M times given that a neighbouring

109 catchment is flooded?"; and (ii) "What is the probability that the overall system fails given that each
110 bridge is designed to a specific exceedance probability event (e.g., the 1% annual exceedance
111 probability event)?" The method for resolving these questions represents a new approach to estimate
112 flood risk for engineering design, by focusing attention on the risk of the entire system, rather than the
113 risk of individual system elements in isolation.

114 In the remainder of the paper, Section 2 emphasises the need for spatially dependent IDF estimates in
115 flood risk design, followed by Section 3 which outlines the case study and data used. Section 4 explains
116 the implementation of the framework, including a method for analysing the spatial dependence of
117 extreme rainfall across different durations. Results on the behaviour of floods due to the spatial and
118 duration dependence of rainfall extremes, are provided in Section 5. Conclusions and discussion follow
119 in Section 6.

120 **2. The need for spatially dependent IDF estimates in flood risk estimation**

121 The main limitation of conventional methods of flood risk estimation is that they isolate bursts of
122 rainfall and break the dependence structure of extreme rainfall. Figure 1 demonstrates a traditional
123 process of estimating at-site extreme rainfall for two locations (gauge 1, gauge 2) and three durations
124 (1, 3, and 5 hr) (Stedinger et al., 1993). The process first involves extracting the extreme burst of rainfall
125 for each site, duration and year from the continuous rainfall data, and then fitting a probability
126 distribution (such as the Generalised Extreme Value (GEV) distribution) to the extracted data. Figure 1
127 demonstrates that, through the process of converting the continuous rainfall data to a series of discrete
128 rainfall 'bursts', this process breaks the dependence both with respect to duration and space. Firstly, the
129 duration dependence is broken by extracting each duration separately, whereas for the hypothetical
130 storm in Fig. 1 it is clear that the annual maxima from some of the extreme bursts come from the same
131 storm. Secondly, the spatial dependence is broken because each site is analysed independently. Again,
132 for the hypothetical storm of Fig. 1 it can be seen that the 5 hr storm has occurred at the same time
133 across the two catchments, and this information is lost in the subsequent probability distribution curves.
134 Lastly, there is cross-dependence in space and duration. For example, the 1 hr extreme from gauge 2
135 occurs at the same time as the 5 hr extreme from gauge 1. This may be relevant if there are two

catchments with times of concentration matching 1 hr and 5 hr respectively, which can arise where catchments are neighbouring or nested.

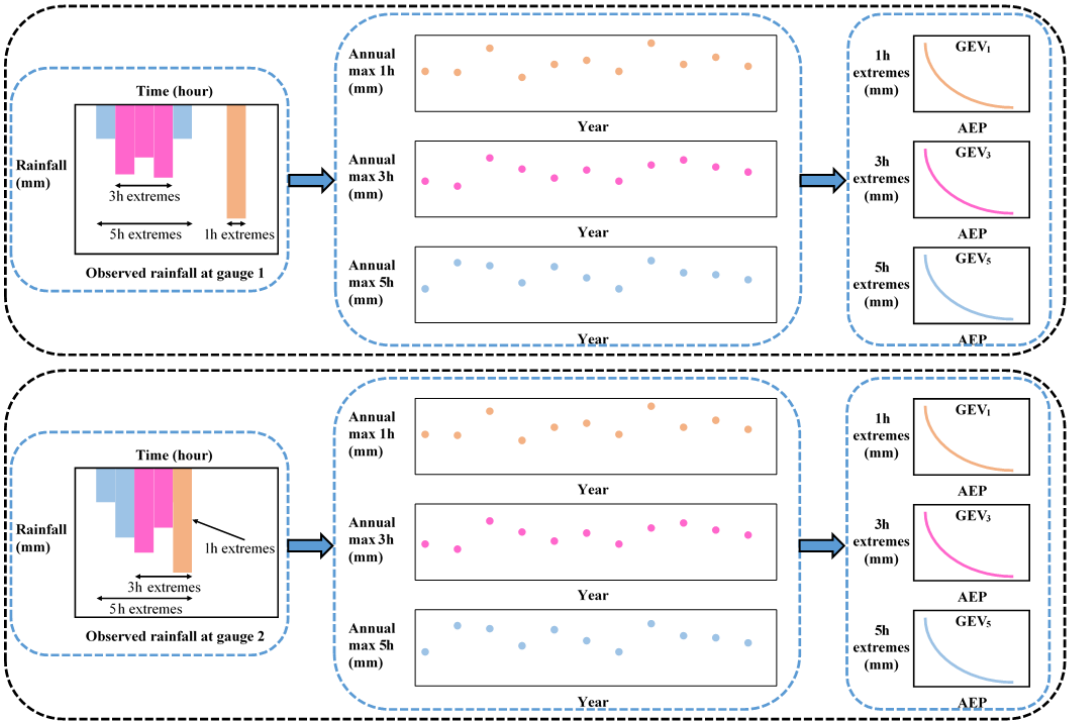

Figure 1. Illustration of process to estimate rainfall extremes for each individual location in conventional flood risk approach, the upper panel is for gauge 1 and the lower panel is for gauge 2.

Having obtained the IDF estimates for individual locations in Fig. 1, the next step is commonly to convert this to spatial IDF maps by interpolating results between gauged locations. Figure 2 shows hypothetical IDF maps from individual sites, with a separate spatial contour map usually provided for each storm burst duration. In a conventional application the respective maps are used to estimate the magnitude of extreme rainfall over catchments for a specified time of concentration. The IDF estimates are combined with an areal reduction factor (ARF) to determine the volume of rainfall over a region (since rainfall is not simultaneously extreme at all locations over the region). However, because the spatial dependence was broken in the IDF analysis, the ARFs come from a separate analysis and are an attempt to correct for the broken spatial relationship within a catchment (Bennett et al., 2016a). Lastly, the rainfall volume over the catchment is combined with a temporal pattern (i.e. the distribution of the rainfall hyetograph within a single 'storm burst') and input to a runoff model to simulate flood-flow at a catchment's outlet. Where catchment flows can be considered independently this process has been

acceptable for conventional design, but because this process does not account for dependence across durations and across a region, it is not possible to address problems that span multiple catchments, as with civil infrastructure systems.

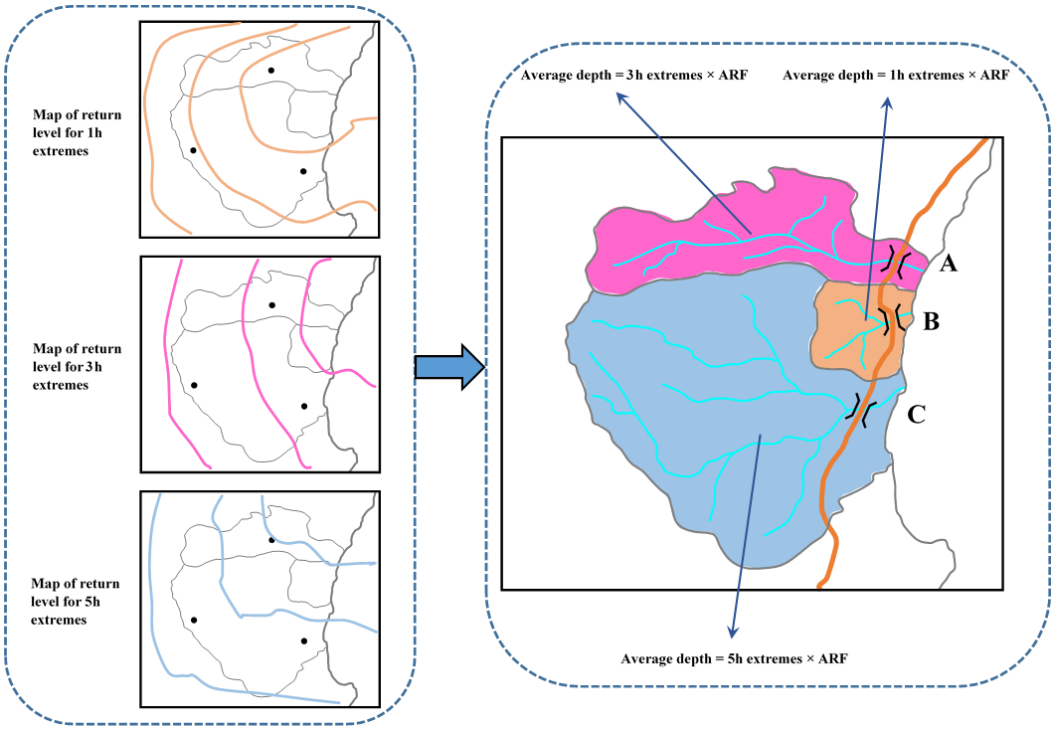

Figure 2. Illustration of map of return level and how to use it in estimating flood flow in conventional flood risk estimates approach.

The process in Fig. 1 breaks out the dependence of the observed rainfall, which makes the conventional approach unable to analyse the dependence of flooding at two or more separate locations. Instead, this paper advocates for spatially dependent IDF estimates that are developed by retaining the dependence of observed rainfall in the estimation of extremal rainfall. By applying spatially dependent IDF estimates to a rainfall-runoff model, it becomes possible to represent the dependence of flooding between separate locations.

3. Case study and data

The region chosen for the case study is in the mid north coast region of New South Wales, Australia. This region has been the focus of a highway upgrade project and has an annual average daily traffic

volume on the order of 15,000 vehicles along the existing highway. The upgrade traverses a series of coastal foothills and floodplains for a total length of approximately 20 km. The project's major river crossings consist of extensive floodplains with some marsh areas.

The case study has five main catchments that are numbered in sequence in Fig. 3: (1) Bellinger, (2) Kalang River, (3) Deep Creek, (4) Nambucca and (5) Warrell Creek. The area and time of concentration of these catchments is summarised in Table 1, with the latter estimated using the ratio of the flow path length and average flow velocity (SKM, 2011). The Deep Creek catchment has a time of concentration of 8 hr, while the other four catchments have much longer times of concentration, ranging from 27 to 38 hr. The differing durations indicate that it is necessary to consider spatial dependence across this range of durations to estimate joint and conditional flood risk. The spatial dependence across rainfall durations is expected to be lower than across a single duration, since short- and long-rain events are often driven by different meteorological mechanisms (Zheng et al., 2015). However some spatial dependence is still likely to be present, given that extremal rainfall in the region is strongly associated with 'east coast low' systems off the eastern coastline, whereby extreme hourly rainfall bursts are often embedded in heavy multi-day rainfall events.

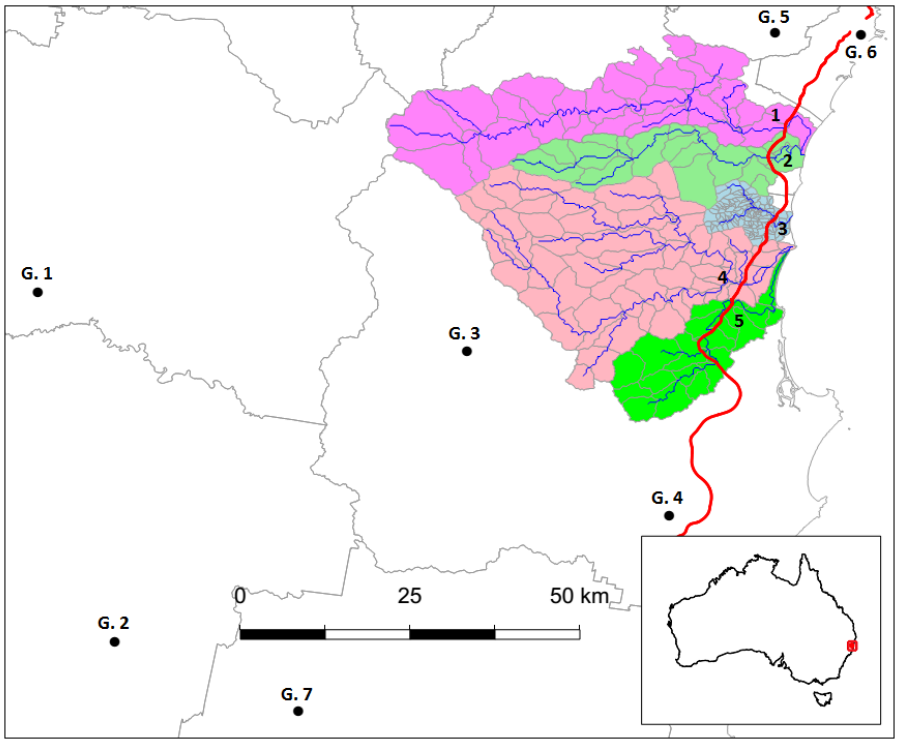

185 **Figure 3.** Map of the case study in New South Wales, Australia. The black dots indicate the rainfall gauges (G. 1 to G. 7),
186 the red line indicates the Pacific Highway upgrade project, and the blue lines indicate the main river network. The numbers
187 from one to five indicate the locations of the main river crossings.

188 **Table 1.** Summary of case study catchments properties .

No.	Catchment	Area (km^2)	Time of concentration (hour)
1	Bellinger	772	37
2	Kalang River	341	33
3	Deep Creek	92	8
4	Nambucca (upper)	1020	38
5	Warrell Creek	294	27

189 The black circles in Fig. 3 represent the sub-daily rain stations used for this study. There were seven
190 sub-daily stations selected, with 35 years of record in common for the whole region. The data was
191 available at a 5 minute interval and aggregated to longer durations. For convenience in comparing the
192 times of concentration between the catchments, this study assumes a time of concentration of 9 hr for
193 the Deep Creek catchment, while identical times of concentration of 36 hr are assumed for the other
194 four catchments.

195

4. Methodology

This section describes the method used to estimate the conditional and joint probabilities of streamflow for civil infrastructure systems based on rainfall extremes, with the sequence of steps illustrated in Fig. 4. The overall aim is to estimate rainfall exceedance probabilities and corresponding flow estimates that account for dependence across multiple catchments. The generalized Pareto distribution (GPD) is used as the marginal distribution to fit to observed rainfall for all durations at each location (Section 4.1). An extremal dependence model is required to evaluate conditional and joint probabilities. Here, an inverted max-stable process is used with dependence not only in space but also in duration (Section 4.2). The fitted model is evaluated in a range of contexts, including the construction of joint and conditional return level maps. The derivation of areal reduction factors and joint rainfall estimates are made with the assistance of simulations based on the fitted model (Section 4.3). An event-based rainfall-runoff model is employed in Section 4.4 to transform extremal design rainfalls to corresponding flows.

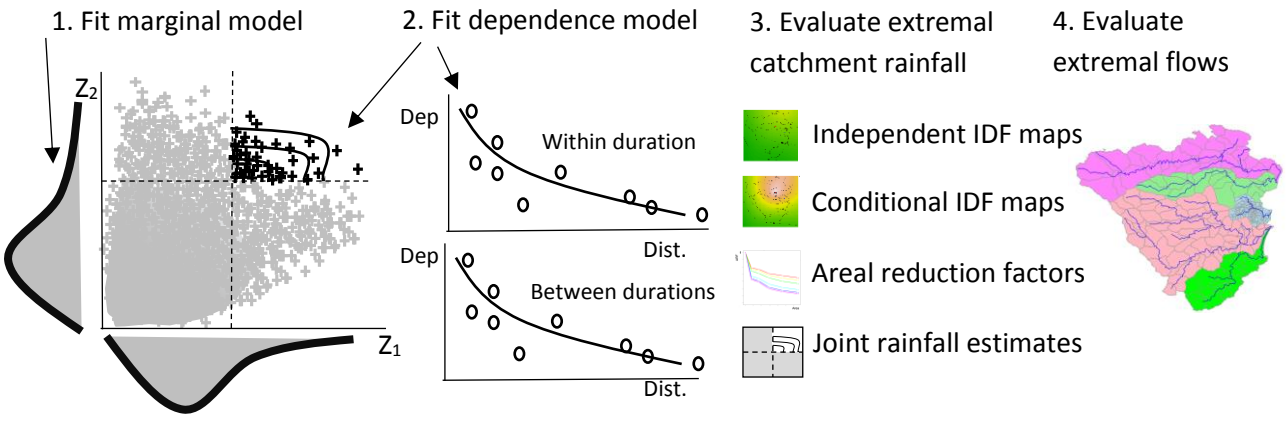

Figure 4. The flow chart for the overall methodology.

4.1. Marginal model for rainfall

This study defines extremes as those greater than some threshold u. For large u, the distribution of Y conditional on $Y > u$ may be approximated by the generalized Pareto distribution (GPD) (Pickands, 1975; Davison and Smith, 1990; Thibaud et al., 2013):

$$G(y) = 1 - \left\{1 + \frac{\xi(y-u)}{\sigma_u}\right\}^{-1/\xi}, \quad y > u, \tag{1}$$

defined on $\{y: 1 + \xi(y-u)/\sigma_u > 0\}$ where $\sigma_u > 0$ and $-\infty < \xi < +\infty$ are scale and shape parameters, respectively. The probability that a level y is exceeded is $\Phi_u\{1 - G(y)\}$, where $\Phi_u = \Pr(Y > u)$.

The selection of the appropriate threshold u involves a trade-off between bias and variance. A threshold that is too low leads to bias because the GPD approximation is poor. A threshold too high leads to high variance because of a small number of excesses. Two diagnostic tests are used to determine the appropriate threshold u: the mean residual life plot and the parameter estimate plot (Coles, 2001; Davison and Smith, 1990). These methods use the stability property of a GPD, so that if a GPD is valid for all excesses above u, then excesses of a threshold greater than u should also follow a GPD (Coles, 2001). To construct IDF maps across the region, the parameters of the GPD are interpolated across the region using a thin plate spline with covariates of longitude and latitude. Though more detailed modelling of covariates could be used to improve estimates (Le et al. 2018b), the interpolation used here is sufficient for demonstrating the overall method.

4.2. Dependence model for spatial rainfall

Consider rainfall as a stationary stochastic process Z_i associated with a location x_i and a specific duration (the notation is simplified from $Z(x_i)$ to Z_i). An important property of dependence in the extremes is whether or not two variables are likely/unlikely to co-occur as the extremes become rarer, as this can significantly influence the estimate of frequency for flood events of large magnitude. This is referred to as asymptotic dependence/independence, respectively. For the case of asymptotic independence, the dependence structure becomes weaker as the extremal threshold increases, which is defined as $\lim_{z\to\infty} P\{Z_1 > z | Z_2 > z\} = 0$ for all $x_1 \neq x_2$. The spatial extent of a rainfall event with asymptotically independent extremes will diminish as its rarity increases. This study uses an asymptotically independent model, of which there are multiple types including the Gaussian copula (Davison et al., 2012) and inverted max-stable processes (Wadsworth and Tawn, 2012). This study uses an inverted Brown-Resnick max-stable process (Asadi et al., 2015; Huser and Davison, 2013; Kabluchko et al., 2009; Oesting et al., 2017) based on a performance evaluation summarised in Le et al. (2018a).

The dependence structure of the inverted max-stable process is represented by the pairwise residual tail dependence coefficient (Ledford and Tawn, 1996). For a generic continuous process Z_i for a given duration and associated with a specific location x_i, the empirical pairwise residual tail dependence coefficient η for each pair of locations (x_1, x_2) is

$$\eta(x_1, x_2) = \lim_{z \to \infty} \frac{\log P\{Z_2 > z\}}{\log P\{Z_1 > z, Z_2 > z\}}. \quad (2)$$

The value of $\eta \in (0,1]$ indicates the level of extremal dependence between Z_1 and Z_2 (Coles et al., 1999), with lower values indicating lower dependence. An example of how to calculate the residual tail dependence coefficient is provided in Appendix A for a sample dataset. To estimate the dependence structure of an inverted max-stable model, the theoretical residual tail dependence coefficient function is fitted to its empirical counterpart. Here the residual tail dependence coefficient function is assumed to only depend on the Euclidean distance between two locations $h = \|x_1 - x_2\|$. The theoretical residual tail dependence coefficient function for the inverted Brown-Resnick model is given as:

$$\eta(h) = \frac{1}{2\Phi\left\{\sqrt{\frac{\gamma(h)}{2}}\right\}}, \quad (3)$$

where Φ is the standard normal cumulative distribution function, h is the distance between two locations, and $\gamma(h)$ belongs to the class of variograms $\gamma(h) = \|h\|^{\beta}/q$ for $q > 0$ and $\beta \in (0,2)$. The model is fitted to the empirical residual tail dependence coefficient by modifying parameters q and β until the sum of squared errors is minimized.

The inverted max-stable process is fitted to the observations by minimizing the sum of the squared errors of the residual tail dependence coefficients. When the extreme rainfall at location x_1 and x_2 are of different durations, the dependence is less than when the extremes are of the same duration. For example, at a single location (h = 0), when the duration is the same, the rainfall values are identical and have perfect dependence, but when the duration of extremes are different the values are not identical and the dependence is less. An adjustment needs to be made to the theoretical pairwise residual tail dependence coefficient function when extreme rainfalls have different durations.

Following Le et al. (2018b), an adjusted approach is used by adding a nugget to the variogram as:

$$\gamma_{ad.}(h) = h^{\beta}/q + c(D-d)/d, \quad (4)$$

where h, β, and q are the same as those in Eq. (3); d is the duration (in hours); $0 < d \leq D$, where D is the maximum duration of interest (e.g. $D = 36$ hr for the case study described in this paper); and c is a parameter to adjust dependence according to duration. This adjustment is intended to condition the behaviour of shorter duration extremes on a D-hour extreme of specified magnitude. It is constructed to reflect the fact that when compared to a D-hour extreme, a shorter duration results in less extremal dependence. Cases involving conditioning of longer periods on shorter periods (such as a 36 hr extreme given a 9 hr extreme has occurred) can also use the relationship in Eq. (4), but with different parameter values.

To fit the inverted max-stable process for all pairs of durations at locations x_1 and x_2 (i.e. 36 hr and 12 hr, 36 hr and 9 hr, 36 hr and 6 hr, 36 hr and 2 hr, 36 hr and 1 hr), the theoretical pairwise residual tail dependence coefficient function in Eq. (3) is used with the adjusted variogram from Eq. (4) where the parameters β and q are first obtained from the fitted results of the case of identical 36 hr durations at location x_1 and x_2. The parameter c is obtained by a least square fit of the residual tail dependence coefficient across all durations.

4.3. Simulation based estimation of areal and joint rainfall

The dependence model specification in the previous section enables the calculation of joint and conditional probabilities (Appendix B). Therefore, in addition to traditional IDF return level maps that are based on independence between locations and durations, it is possible to account for the coincidence of rainfall within the region. Current design procedures using IDF estimates are event-based and rely on ancillary steps to reconstruct elements of the design storm that were broken during the estimation procedure. One critical element is the areal reduction factor (ARF), which the dependence model can also be used to estimate. ARFs are used to adjust rainfall at a point (such as the centroid of a catchment) to an effective mean rainfall over the catchment with equivalent probability of exceedance (Ball et al., 2016; Le et al., 2018a). ARFs can be estimated from observed rainfall data, but it is difficult to

292 extrapolate them for long return periods from observations with just 35 years of record for this study.
293 To deal with this difficulty and to analyse the asymptotic behaviour of ARFs, Le et al. (2018a) proposed
294 a framework to simulate ARFs using the same inverted-max stable process model adopted here. The
295 simulation procedure from Le et al. (2018a) is summarised according to two steps. In the first step, the
296 theoretical residual tail dependence coefficient function in Eq. (3) is fitted to observed rainfall for the
297 duration of interest to obtain the variogram parameters $q > 0$ and $\beta \in (0,2)$. The inverted Brown-
298 Resnick process is obtained from a simulation of the Brown-Resnick process using the algorithm of
299 Dombry et al. (2016) over a spatial domain. In the second step, the simulation in step 1 is transformed
300 from unit Fréchet margins to the rainfall scaled margins (inverse transformation of Eq. (B.1) in
301 Appendix B). For rainfall magnitudes above the threshold the generalised Pareto distribution in Eq. (1)
302 is used, and below the threshold the empirical distribution is used. The empirical distributions at
303 ungauged sites are derived from the nearest gauged sites and using the interpolated response surface of
304 the GPD threshold parameter.

305 An advantage of the simulation approach is that it can reflect the proportion of dry days in the empirical
306 distribution by making the simulated rainfall contain zero values (Thibaud et al., 2013). Another
307 advantage is that the use of empirical distributions guarantees that the marginal distributions of
308 simulated rainfall below the threshold match the observed marginal distributions. There may be a
309 drawback by forcing the simulated rainfall to have the same extremal dependence structure for both
310 parts below and above the threshold, which may not be true for non-extreme rainfall. However, the
311 dependence structure of non-extreme rainfall contributes insignificantly to extreme events (Thibaud et
312 al., 2013) and is unlikely to affect the results.

313 For calculating ARFs, the simulation is implemented separately for spatial rainfall of 36 and 9 hrs
314 duration. ARFs are calculated for each duration and different return periods, which can be found in the
315 supplementary material (Fig. S1 and S2). Figure S1 and S2 provide relationships between ARFs and
316 area (in km^2) for different return periods for the case study catchments simulated using the inverted
317 Brown-Resnick process over equally sized grid points. The relationships are interpolated to obtain the
318 ARFs for each subcatchment.

The recommended approach for estimating the overall failure probability of a system is demonstrated by considering a hypothetical traffic system with multiple river crossings at locations. If there is a one-to-one correspondence between extreme rainfall intensity over a catchment and flood magnitude, the overall failure probability will be approximately equal to the probability that there is at least one river crossing whose contributing catchment has rainfall extremes exceeding the design level, which can be estimated using simulations of the spatial rainfall model. Given the different times of concentration in each catchment, the simulation must account for extremes of different durations. Specifically, the covariance matrix of the simulation procedure provided by Dombry et al. (2016) is calculated from the variogram in Eq. (3). The covariance element for a pair of locations with the same duration (e.g. 36 and 36 hr) is calculated from the variogram of identical durations for 36 and 36 hr. The covariance element for a pair of locations with different durations, for example 36 and 9 hr, is calculated from the variogram across durations for 36 and 9 hr. A set of 10,000 years simulated rainfall is generated from the fitted model to calculate the overall failure probability of a highway section (Eq. B.5). The process is repeated 100 times to estimate the average failure probability, under the assumption that all river crossings of the highway are designed to the same individual failure probability.

4.4. Transforming rainfall extremes to flood flow

To estimate flood flow from rainfall extremes, the Watershed Bounded Network Model (WBNM) (Boyd et al., 1996), is employed. WBNM calculates flood runoff from rainfall hyetographs that represent the relationship between the rainfall intensity and time (Chow et al., 1988). It divides the catchment into subcatchments, allowing hydrographs to be calculated at various points within the catchment, and allowing the spatial variability of rainfall and rainfall losses to be modelled. It separates overland flow routing from channel routing, allowing changes to either or both of these processes, for example in urbanised catchments. The rainfall extremes are estimated at the centroid of the catchment, and are converted to average spatial rainfall using the simulated ARFs described in Section 4.3. Design rainfall hyetographs are used to convert the rainfall magnitude to absolute values through the duration of a storm following standard design guidance in Australia (Ball et al., 2016).

Hydrological models (WBNM) for the case study area were developed and calibrated in previous studies (WMAWater, 2011). Hydrological model layouts for the Bellinger, Kalang River, Nambucca, Warrell and Deep Creek catchments can be found in the supplementary material (Fig. S3 to S5).

5. Results

5.1. Evaluation of model for space-duration rainfall process

A GPD with an appropriate threshold was fitted to the observed rainfall data for 36 hr and 9 hr durations, and the Brown-Resnick inverted max-stable process model was calibrated to determine the spatial dependence.

Analysis of the rainfall records led to the selection of a threshold of 0.98 for all records as reasonable across the spatial domain and the GPD was fitted to data above the selected threshold. Figure 5 shows QQ plots of the marginal estimates for a representative station for two durations (36 and 9 hr). Overall the quality of fitted distributions is good and plots for all other stations can be found in the supplementary material (Fig. S6 and S7).

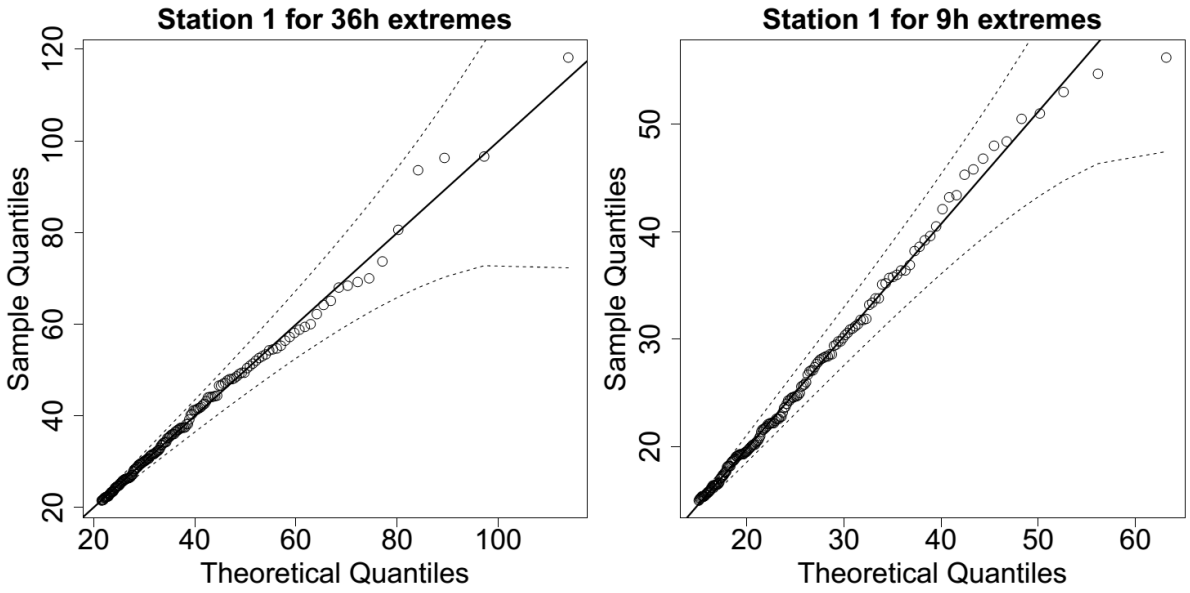

Figure 5. QQ plots for the fitted GPD at one representative station, dotted lines are the 95% confidence bounds, and the solid diagonal line indicates a perfect fit.

The inverted max-stable process across different durations was calibrated to determine dependence parameters. The theoretical pairwise residual tail dependence coefficient function between two

363 locations (x_1 and x_2) was calculated based on Eq. (3) and Eq. (4), and the observed pairwise residual
364 tail dependence coefficient η was calculated using Eq. (2). Figure 6 shows the pairwise residual tail
365 dependence coefficients for the Brown-Resnick inverted max-stable process versus distance. The black
366 points are the observed pairwise residual tail dependence coefficients, while the red lines are the fitted
367 pairwise residual tail dependence coefficient functions. A coefficient equal to 1 indicates complete
368 spatial dependence, and a value of 0.5 indicates complete spatial independence. The top-left panel
369 shows the dependence between 36 hr extremes across space, with the distance h = 0 corresponding to
370 "complete dependence". It also shows the dependence decreasing with increasing distance. Figure 6
371 indicates that the model has a reasonable fit to the observed data given the small number of dependence
372 parameters. Although the theoretical coefficient (red line) does not perfectly match at long distances,
373 the main interest for this case study is in short distances, including at $h = 0$ for the case of dependence
374 between two different durations at the same location.

375 The remaining panels of Fig. 6 show the dependence of 36 vs. 9 hr extremes, 36 vs. 6 hr extremes, and
376 36 vs. 3 hr extremes, with the latter two duration combinations not being used directly in the study but
377 nonetheless showing the model performance across several durations. As expected, the dependence
378 levels are weaker compared with 36 vs. 36 hr extremes at the same distance, especially at zero distance.
379 This is expected, as extremes of different durations are more likely to arise from different storm events
380 compared to storms of the same duration.

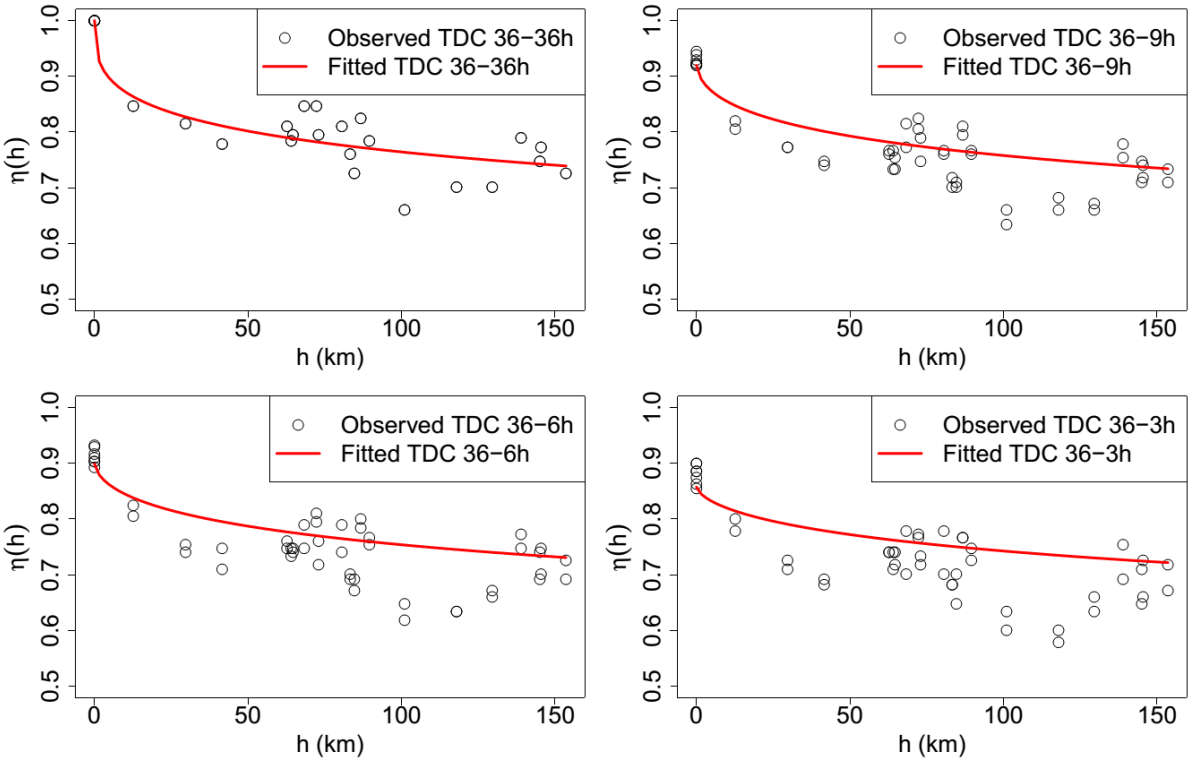

Figure 6. Plots of pairwise residual tail dependence coefficient (TDC) against distance for 36 hr extremes and 36 hr extremes (top left), for 36 hr extremes and 9 hr extremes (top right), for 36 hr extremes and 6 hr extremes (bottom left), and for 36 hr extremes and 3 hr extremes (bottom right). The black points are estimated residual tail dependence coefficients for pairs of sub-daily stations, and the red lines are theoretical residual tail dependence coefficient function.

5.2. Estimating conditional rainfall return levels and corresponding conditional flows for evacuation route design

The recommended approach for estimating conditional rainfall extremes is demonstrated by considering a hypothetical evacuation route across location x_2, given a flood occurs at location x_1, evaluated using Eq. (B.4). This approach is applied to a case study of the Pacific Highway upgrade project that contains five main river crossings (from Fig. 3). For evacuation purposes, we need to know "what is the probability that a bridge fails only once on average every M times (e.g., $M = 10$ for a one in 10 chance conditional event) when a neighbouring bridge is flooded?" This section provides the conditional estimates for two pairs of neighbouring bridges in the case study that have the shortest Euclidean distances, i.e. pairs (x_1, x_2) and (x_2, x_3). The comparisons of unconditional and conditional maps are given in Fig. 7 and Fig. 8, and the corresponding unconditional and conditional flows are given in Fig. 9.

The left panel of Fig. 7 provides the pointwise 10-year unconditional return level map over the case study area for 36 hr rainfall extremes. The value at the location of interest—the blue star (the centroid of Bellinger catchment)—is around 260 mm. The right panel of Fig. 7 indicates that when accounting for the effect of a 20-year event for 36 hr rainfall extremes happening at the location of the red star (the centroid of Kalang River catchment), the pointwise one in 10 chance conditional return level at the blue star rises to around 453 mm (i.e., 1.74 times the unconditional value).

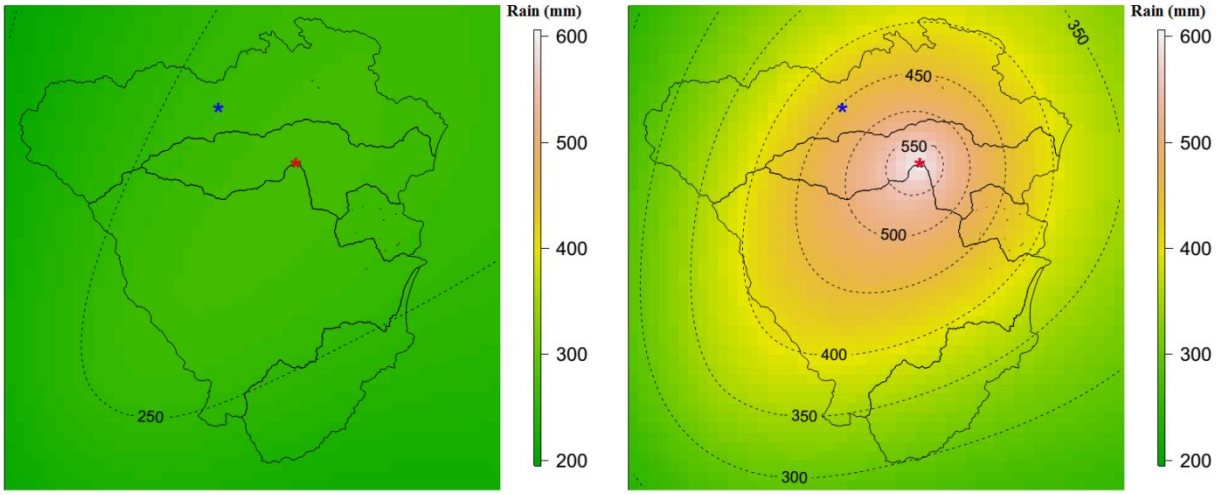

Figure 7. Pointwise 10-year unconditional return level map (mm) for 36 hr extremes (left), and pointwise one in 10 chance conditional return level map (mm) for 36 hr extremes given a 20-year event for 36 hr extremes happen at location of the red star for the centroid of Kalang River catchment (right). The colour scales are the same for comparison.

Figure 8 provides similar plots to Fig. 7 for another pair of locations having different durations of rainfall extremes due to different times of concentration in each catchment. Here, the location of interest is the centroid of the Deep Creek catchment (the blue star in Fig. 8) and the conditional point is the centroid of the Kalang River catchment (the red star in Fig. 8). The pointwise 10-year unconditional and one in 10 chance conditional return levels at the location of the blue star are 134 mm and 194 mm, respectively. The relative difference between the conditional and unconditional return levels is only 1.45 times, compared with 1.74 times for the case in Fig. 7. This is because the pair of locations in Fig. 8 has a longer distance than those in Fig. 7, so that the dependence level is weaker. Moreover, the location pair in Fig. 8 was analysed for different durations (between 36 and 9 hr extremes), which has

weaker dependence than the case of the equivalent durations in Fig. 7 (between 36 and 36 hr), based on Fig. 6.

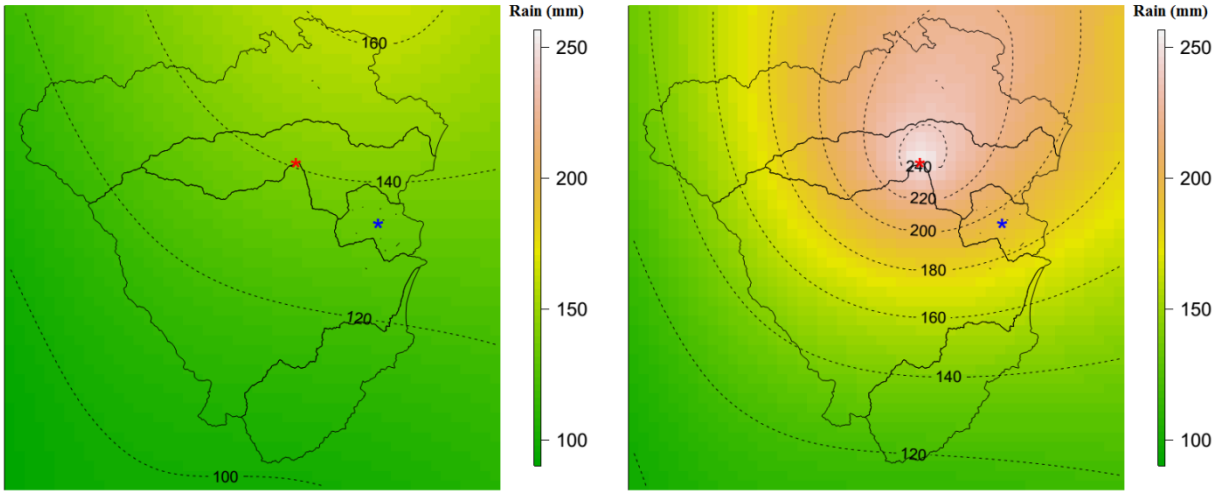

Figure 8. Pointwise 10-year unconditional return level map (mm) for 9 hr extremes (left), and pointwise one in 10 chance conditional return level map (mm) for 9 hr extremes, given a 20-year event for 36 hr extremes happens at location of the red star for the centroid of the Kalang River catchment (right). The colour scales are the same for comparison.

The unconditional and conditional return levels were extracted at the centroid of each main catchment, and were converted to the absolute values of rainfall using a corresponding ARF and design storm hyetograph. The unconditional and conditional flood flows at the river crossing in the Bellinger catchment (corresponding to the unconditional and conditional rainfall extremes in Fig. 7) are given in Fig. 9 (left panel). Similar plots for the river crossing in the Deep Creek catchment (corresponding to the unconditional and conditional rainfall extremes in Fig. 8) are given in Fig. 9 (right panel).

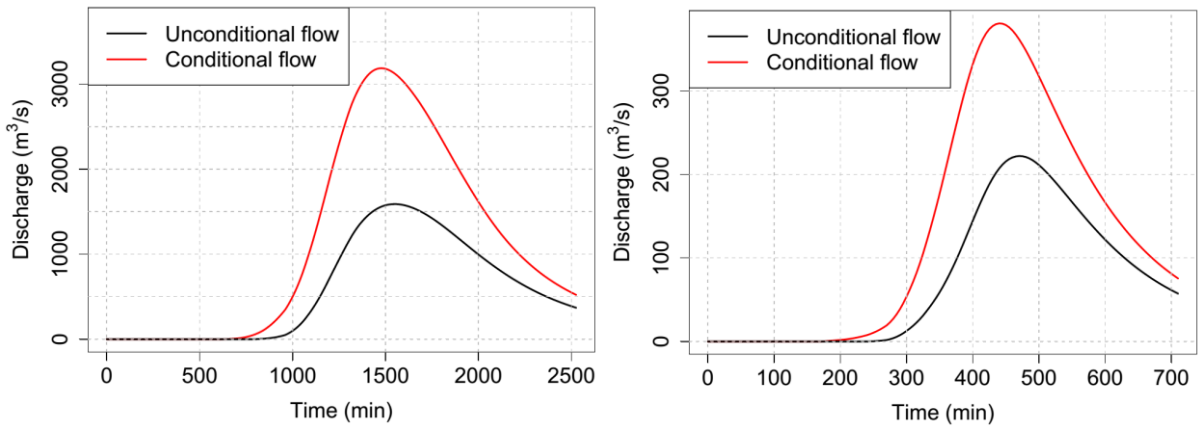

Figure 9. Comparison between conditional flows (red line) and unconditional flows (black line). (left) At the river crossing in the Bellinger catchment (number 1 in Figure 3): conditional flow caused by an one in 10 chance conditional event for 36 hr rainfall in considering the effect of a 20-year event for 36 hr rainfall occurring at the river crossing in the Kalang River catchment, and unconditional flow caused by a 10-year unconditional event for 36 hr. (right) At the river crossing in the Deep Creek catchment (number 3 in Figure 3): conditional flow caused by an one in 10 chance conditional event for 9 hr rainfall in considering the effect of a 20-year event for 36 hr rainfall occurring at the river crossing in the Kalang River catchment, and unconditional flow caused by a 10-year unconditional event for 9 hr rainfall.

Fig. 9 presents peak flow for the Bellinger (left panel) and Deep Creek (right panel) catchments, indicating that the peak conditional flow at the river crossings is almost 2.0 and 1.7 times higher than the unconditional flow for the two catchments, respectively. This difference is a direct result of the conditional event having a higher rainfall magnitude than the unconditional event: given that there is an extreme event nearby, it is more likely for an extreme event to occur at a nearby location. If a bridge design were to take into account this extra criterion for the purposes of evacuation planning it would require the design to be at a higher level.

5.3. Estimating the failure probability of the highway section based on the joint probability of rainfall extremes

Figure 10 is a plot of the overall failure probability of the highway as a function of the failure probability of each individual river crossing (black). Similar relationships for the cases of complete dependence (blue) and independence (red) are also provided for comparison. For the case of complete dependence, when the whole region is extreme at the same time, the overall failure probability of the highway is equal to the individual river crossing failure probability and it represents the lowest overall failure probability. The worst case is complete independence where extremes do not happen together unless by random chance; this means the failure probability of the highway is much higher than that for individual river crossings. Taking into account the real dependence, there are some extremes that align and it seems from Fig. 10 that this is a relatively weak effect. As an example from Fig. 10, to design the highway with a failure probability of 1% annual exceedance probability (AEP), we would have to design each individual river crossing to a much rarer AEP of 0.25% (see green lines in Fig. 10).

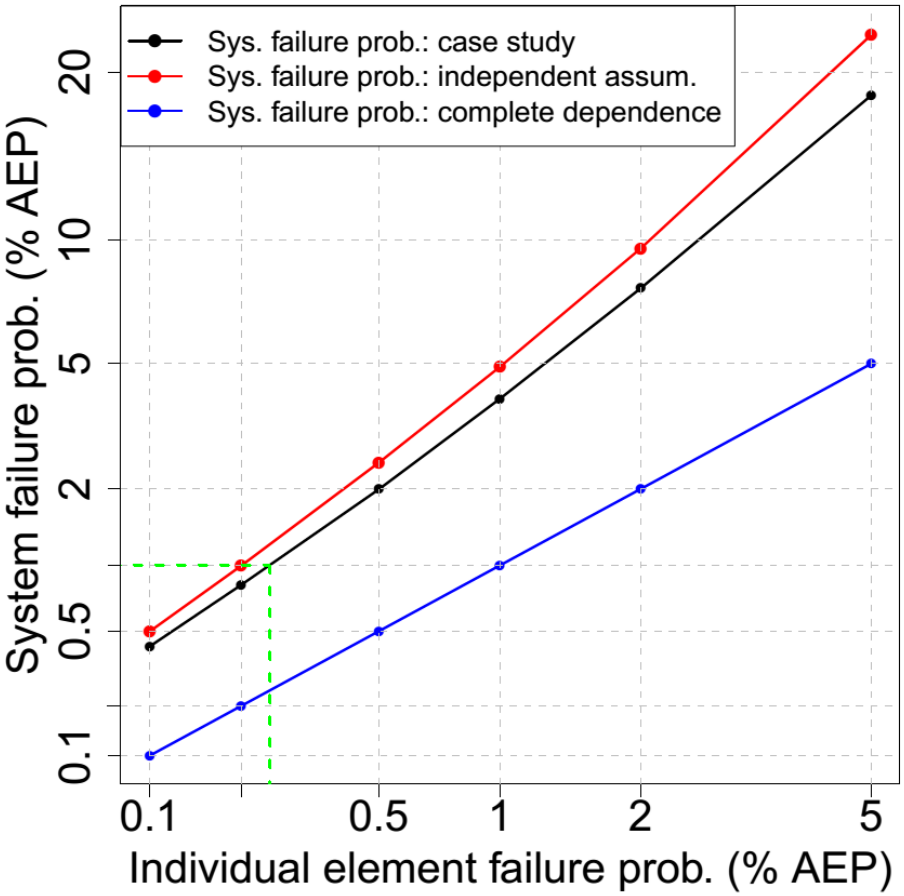

Figure 10. Relationship between system failure probability and individual element failure probability in % annual exceedance probability (% AEP). The black colour is for the case study, the red colour is for the case of independence, and the blue colour is for the case of complete dependence. The green lines help to interpolate the individual element failure probability from a given system failure probability of 1%. Both horizontal axis and vertical axis are constructed at a double log scale for viewing purposes.

6. Discussion and Conclusions

Hydrological design that is based on IDF estimates has conventionally focussed on separate estimation at single locations. Such an approach can lead to the misspecification of wider system risk of flooding since weather systems exhibit dependence in space, time and across storm durations, which can lead to the coincidence of extremes. A number of methods have been developed to address the problem of antecedent moisture within a single catchment, by accounting for the temporal dependence of rainfall at locations of interest through loss parameters or sampling rainfall patterns (Rahman et al., 2002). However, there have been fewer methods that account for the spatial dependence of rainfall across

multiple catchments, due in part to the complexity of representing the effects of spatial dependence in risk calculations. Different catchments can have different times of concentration, so spatial dependence may also imply the need to consider dependence across different durations of extreme rainfall bursts.

Recent and ongoing advances in modelling spatial rainfall extremes provide an opportunity to revisit the scope of hydrological design. Such models include a max-stable model fitted using a Bayesian hierarchical approach (Stephenson et al., 2016), max-stable and inverted max-stable models (Nicolet et al., 2017; Padoan et al., 2010; Russell et al., 2016; Thibaud et al., 2013; Westra and Sisson, 2011) and latent-variable Gaussian models (Bennett et al., 2016b). The ability to simulate rainfall over a region means that hydrological problems need not be confined to individual catchments, but may cover multiple catchments. Civil infrastructure systems such as highways, railways or levees are such examples, since the failure of any one element may lead to overall failure of the system. Alternatively, where there is a network, the failure of one element may have implications for the overall system to accommodate the loss, by considering alternative routes. With models of spatial dependence and duration dependence of extremes, there is a new and improved ability to address these problems explicitly as part of the design methodology.

This paper demonstrated an application for evaluating conditional and joint probabilities of flood at different locations. This was achieved with two examples: (i) the design of a river crossing that will fail once on average every M times given that its neighbouring river crossing is flooded; and (ii) estimating the probability that a highway section, which contains multiple river crossings, will fail based on the failure probability of each individual river crossing. Due to the lack of continuous streamflow data and sub-daily limitations of rain-based continuous simulation, this study used an event-based method of conditional and joint rainfall extremes to estimate the corresponding conditional and joint flood flows. The spatial rainfall was simulated using an asymptotically independent model, which was then used to estimate conditional and joint rainfall extremes. An empirical method was obtained from the framework of Le et al. (2018b) to make an asymptotically independent model—the inverted max-stable process—able to capture the spatial dependence of rainfall extremes across different durations. The fitted residual tail dependence coefficient function showed that the model can capture the dependence for different

500 pairs of durations. For our example, the highest ratio of the one in 10 chance conditional event (in
501 considering the effect of a 20-year event rainfall occurring at the conditional location) to the 10-year
502 unconditional event was 1.74, for the two catchments having the strongest dependence (Fig. 7). The
503 corresponding conditional flows were then estimated using a hydrological model WBNM and shown
504 to be strongly related to the ratio of conditional and unconditional rainfall extremes (Fig. 9).

505 The joint probability of rainfall extremes for all catchments and for all possible pairs of catchments in
506 the case study area was estimated empirically from a set of 10,000 years of simulated rainfall extremes,
507 repeated 100 times to estimate the average value. The results showed that there were differences in the
508 failure probability of the highway after taking into account the rainfall dependence, but the effect was
509 not as emphatic as with the case of conditional probabilities. The difference in the failure probability
510 became weaker as the return period increased, which is consistent with the characteristic of
511 asymptotically independent data (Ledford and Tawn, 1996; Wadsworth and Tawn, 2012). A
512 relationship was demonstrated (Fig. 10) to show how the design of the overall system to a given failure
513 probability requires the design of each individual river crossing to a rarer extremal level than when each
514 crossing is considered in isolation. For the case study example, it would be necessary to design each of
515 the five bridges to a 0.25% AEP event in order to obtain a system failure probability of 1%.

516 There is a need to reimagine the role of intensity-duration-frequency relationships. Conventionally they
517 have been developed as maps of the marginal rainfall in a point-wise manner for all locations and for a
518 range of frequencies and durations. The increasing sophistication of mathematical models for extremes,
519 computational power and interactive graphics abilities of online mapping platforms means that analysis
520 of hydrological extremes could significantly expand in scope. With an underlying model of spatial and
521 duration dependence between the extremes, it is not difficult to conceive of digital maps that
522 dynamically transform from the marginal representation of extremes to the corresponding
523 representation conditional extremes after any number of conditions are applied. This transformation is
524 exemplified by the differences between left and right panels in Fig. 7 and Fig. 8. Enhanced IDF maps
525 would enable a very different paradigm of design flood risk estimation, breaking away from analysing
526 individual system elements in isolation and instead emphasizing the behaviour of entire system.

Appendix A. Calculation of empirical tail dependence coefficient

To illustrate how Eq. (2) in the manuscript is calculated, consider a set of $n = 10$ observed values at the two locations: Z_1 and Z_2 (see Table A1). First, Z_1 and Z_2 are converted to empirical cumulative probability estimates via the Weibull plotting position formula $P = j/(n+1)$ where j is ranked index of a data point giving P_1 and P_2 (see Table A1).

Table A1. Observed data Z_1 and Z_2 and corresponding empirical cumulative probabilities P_1 and P_2.

$\boldsymbol{Z_1}$	$\boldsymbol{Z_2}$	$\boldsymbol{P_1}$	$\boldsymbol{P_2}$
5	10	0.455	0.909
9	1	0.818	0.091
1	7	0.091	0.636
2	6	0.182	0.545
10	4	0.909	0.364
3	3	0.273	0.273
8	9	0.727	0.818
6	2	0.545	0.182
4	8	0.364	0.727
7	5	0.636	0.455

Assume that interest is in values above a threshold u satisfying $P_u = 0.5$, in other words, $P\{Z_2 > u\} = P\{P_2 > P_u\} = 0.5$. In this case we have only one pair, at the index of 7, that satisfy both P_1 and P_2 are greater than $P_u = 0.5$, thus $P\{Z_1 > u, Z_2 > u\} = P\{P_1 > P_u, P_2 > P_u\} = 1/10 = 0.1$. The calculation of the empirical tail dependence coefficient is then

$$\eta(x_1, x_2) = \frac{\log P\{Z_2 > u\}}{\log P\{Z_1 > u, Z_2 > u\}} = \frac{\log P\{P_2 > P_u\}}{\log P\{P_1 > P_u, P_2 > P_u\}} = \frac{\log(0.5)}{\log(0.1)} = 0.301. \qquad (A.1)$$

Appendix B Estimate of conditional and joint probabilities of rainfall extremes

The unit Fréchet transformation is given as

$$z = \begin{cases} \left(log\left\{1 - \Phi_u\left(1 + \frac{\xi(y-u)}{\sigma_u}\right)^{-1/\xi}\right\}\right)^{-1} & y > u, \xi \neq 0 \\ -\left(log\left\{1 - \Phi_u exp\left(-\frac{y-u}{\sigma_u}\right)^{-1/\xi}\right\}\right)^{-1} & y > u, \xi = 0 \\ -\{logF(y_i)\}^{-1} & y \leq u \end{cases} \quad (B.1)$$

where y is the original marginal value and z is the Fréchet transformed value and all other parameters correspond to the GPD specified in Section 4.1. For values below the threshold, F is the empirical distribution function of y, $F(y_i) = i/(n+1)$ where i is the rank of y_i and n is the total number of data points.

The conditional probability $P\{Z_2 > z_2 | Z_1 > z_1\}$ is obtained from the bivariate inverted max-stable process cumulative distribution function (CDF) in unit Fréchet margins (Thibaud et al., 2013), which is given as:

$$P\{Z_1 \leq z_1, Z_2 \leq z_2\} = 1 - \exp\left\{-\frac{1}{g_1}\right\} - \exp\left\{-\frac{1}{g_2}\right\} + \exp[-V\{g_1, g_2\}], \quad (B.2)$$

where $g_1 = -1/\log\{1 - \exp(-1/z_1)\}$, $g_2 = -1/\log\{1 - \exp(-1/z_2)\}$, and the exponent measure V (Padoan et al., 2010) is defined as:

$$V\{g_1, g_2\} = -\frac{1}{g_1}\Phi\left\{\frac{a}{2} + \frac{1}{a}log\frac{g_2}{g_1}\right\} - \frac{1}{g_2}\Phi\left\{\frac{a}{2} + \frac{1}{a}log\frac{g_1}{g_2}\right\}. \quad (B.3)$$

In Eq. (B.3), Φ is the standard normal cumulative distribution function, $a = \sqrt{2\gamma_{ad.}(h)}$ with $\gamma_{ad.}(h)$ is the variograms that was mentioned in the explanation of Eq. (3).

In unit Fréchet margins, the relationship between the return level z and the return period T (in number of observations) is given as $z = -1/log(1 - 1/T)$, and the conditional probability for the max-stable process can then be estimated using:

$$P\{Z_2 > z_2 | Z_1 > z_1\} = T_1\left[\frac{1}{T_1} - \exp\left(-\frac{1}{z_2}\right) + P\{Z_1 \leq z_1, Z_2 \leq z_2\}\right], \quad (B.4)$$

where T_1 is the return period (in number of observations for 36 hr rainfall) corresponding to the return level z_1. It is also noted that in this paper Z_1 and Z_2 were taken as threshold exceedances, so the return period T_1 should be in the number of observations, which is equivalent to a $T_1/243$−year return period because there are 243 observations for 36 hr rainfall in a year.

The probability that there is at least one location that has an extreme event exceeding a given threshold can be calculated based on the addition rule for the union of probabilities, as:

$$P(Z_1 > z_1 \text{ or } \dots \text{ or } Z_N > z_N) = \sum_{i=1}^{N} P(Z_i > z_i) - \sum_{i<j} P\big(Z_i > z_i, Z_j > z_j\big) + \cdots$$

$$+(-1)^{N-1} P(Z_1 > z_1, \dots, Z_N > z_N), \qquad (B.5)$$

where N is the number of locations.

For the case of dependent variables, the joint probability for only two locations $P\{Z_1 > z_1, Z_2 > z_2\}$ can be easily obtained from the bivariate CDF for inverted max-stable process in Eq. (B.2). However, for the case of multiple locations (five different locations for this paper), it is difficult to derive the formula for this probability because there are dependences between extreme events at all locations. So this probability is empirically calculated from a large number of simulations of the dependent model (see the description of the simulation procedure for an inverted max-stable process in Section 4.3).

For the case that all of events are independent, the joint probability for independent variables is broken down as the product of the marginals, and the conditional probability is equivalent to the marginal probability. When applying Eq. (B.5) for independent variables, the joint probability is therefore calculated by $P(Z_1 > z_1, \dots, Z_N > z_N) = P(Z_1 > z_1) \dots P(Z_N > z_N)$.

Acknowledgments

The lead author was supported by the Australia Awards Scholarships (AAS) from Australia Government. A/Prof Westra was supported by Australian Research Council Discovery grant DP150100411. We thank Mark Babister and Isabelle Testoni of WMA Water for providing the hydrologic models for the case study; and Leticia Mooney for her editorial help in improving this

583 manuscript. The rainfall data used in this study were provided by the Australian Bureau of Meteorology,
584 and can be obtained from the corresponding author.

585 **References**

586 Asadi, P., Davison, A. C., and Engelke, S.: Extremes on river networks, Ann. Appl. Stat., 9, 2023-2050,
587 10.1214/15-AOAS863, 2015.
588 Ball, J., Babister, M., Nathan, R., Weeks, W., Weinmann, E., Retallick, M., and Testoni, I.: Australian
589 Rainfall and Runoff: A Guide to Flood Estimation, © Commonwealth of Australia (Geoscience
590 Australia), 2016.
591 Bárdossy, A., and Pegram, G. G. S.: Copula based multisite model for daily precipitation simulation,
592 Hydrol. Earth Syst. Sci., 13, 2299-2314, 10.5194/hess-13-2299-2009, 2009.
593 Baxevani, A., and Lennartsson, J.: A spatiotemporal precipitation generator based on a censored latent
594 Gaussian field, Water Resources Research, 51, 4338-4358, doi:10.1002/2014WR016455, 2015.
595 Bennett, B., Lambert, M., Thyer, M., Bates, B. C., and Leonard, M.: Estimating Extreme Spatial
596 Rainfall Intensities, Journal of Hydrologic Engineering, 21, 04015074, doi:10.1061/(ASCE)HE.1943-
597 5584.0001316, 2016a.
598 Bennett, B., Thyer, M., Leonard, M., Lambert, M., and Bates, B.: A comprehensive and systematic
599 evaluation framework for a parsimonious daily rainfall field model, Journal of Hydrology,
600 https://doi.org/10.1016/j.jhydrol.2016.12.043, 2016b.
601 Bernard, M. M.: Formulas for rainfall intensities of long duration, Transactions of the American Society
602 of Civil Engineers, 96, 592-606, 1932.
603 Boughton, W., and Droop, O.: Continuous simulation for design flood estimation—a review,
604 Environmental Modelling & Software, 18, 309-318, https://doi.org/10.1016/S1364-8152(03)00004-5,
605 2003.
606 Boyd, M. J., Rigby, E. H., and VanDrie, R.: WBNM — a computer software package for flood
607 hydrograph studies, Environmental Software, 11, 167-172, https://doi.org/10.1016/S0266-
608 9838(96)00042-1, 1996.
609 Brown, B. M., and Resnick, S. I.: Extreme Values of Independent Stochastic Processes, Journal of
610 Applied Probability, 14, 732-739, 10.2307/3213346, 1977.
611 Cameron, D. S., Beven, K. J., Tawn, J., Blazkova, S., and Naden, P.: Flood frequency estimation by
612 continuous simulation for a gauged upland catchment (with uncertainty), Journal of Hydrology, 219,
613 169-187, https://doi.org/10.1016/S0022-1694(99)00057-8, 1999.
614 Carreau, J., Neppel, L., Arnaud, P., and Cantet, P.: Extreme Rainfall Analysis at Ungaug ed Sites in the
615 South of France : Comparison of Three Approaches, Jour nal de la Société Française de Statistique, 154
616 No. 2, 119-138, 2013.
617 Chow, V. T., Maidment, D. R., and Mays, L. W.: Applied Hydrology, McGraw-Hill, c1988, New York,
618 1988.
619 Coles, S., Heffernan, J., and Tawn, J.: Dependence Measures for Extreme Value Analyses, Extremes,
620 2, 339-365, 10.1023/a:1009963131610, 1999.
621 Coles, S.: An Introduction to Statistical Modeling of Extreme Values, Springer Series in Statistics,
622 Springer, 2001.
623 Davison, A. C., and Smith, R. L.: Models for exceedances over high thresholds, Journal of the Royal
624 Statistical Society. Series B (Methodological), 393-442, 1990.
625 Davison, A. C., Padoan, S. A., and Ribatet, M.: Statistical Modeling of Spatial Extremes, Statistical
626 Science, 161-186, 10.1214/11-STS376, 2012.
627 de Haan, L.: A Spectral Representation for Max-stable Processes, The Annals of Probability, 12, 1194-
628 1204, 10.2307/2243357, 1984.
629 Demarta, S., and McNeil, A. J.: The t Copula and Related Copulas, International Statistical Review /
630 Revue Internationale de Statistique, 73, 111-129, 2005.
631 Dombry, C., Engelke, S., and Oesting, M.: Exact simulation of max-stable processes, Biometrika, 103,
632 303-317, 2016.

Durocher, M., Chebana, F., and Ouarda, T. B. M. J.: On the prediction of extreme flood quantiles at ungauged locations with spatial copula, Journal of Hydrology, 533, 523-532, https://doi.org/10.1016/j.jhydrol.2015.12.029, 2016.
Favre, A. C., Adlouni, S. E., Perreault, L., Thiémonge, N., and Bobée, B.: Multivariate hydrological frequency analysis using copulas, Water Resources Research, 40, doi:10.1029/2003WR002456, 2004.
Gupta, A. S., and Tarboton, D. G.: A tool for downscaling weather data from large-grid reanalysis products to finer spatial scales for distributed hydrological applications, Environmental Modelling & Software, 84, 50-69, https://doi.org/10.1016/j.envsoft.2016.06.014, 2016.
He, Y., Bárdossy, A., and Zehe, E.: A review of regionalisation for continuous streamflow simulation, Hydrology and Earth System Sciences, 15, 3539, 2011.
Hegnauer, M., Beersma, J., Van den Boogaard, H., Buishand, T., and Passchier, R.: Generator of Rainfall and Discharge Extremes (GRADE) for the Rhine and Meuse basins; Final report of GRADE 2.0, Document extern project, 2014.
Hosking, J. R. M., and Wallis, J. R.: Regional Frequency Analysis - An Approach Based on L-Moments, Cambridge University Press, Cambridge, UK, 1997.
Huser, R., and Davison, A. C.: Composite likelihood estimation for the Brown–Resnick process, Biometrika, 100, 511-518, 10.1093/biomet/ass089, 2013.
Hüsler, J., and Reiss, R.-D.: Maxima of normal random vectors: Between independence and complete dependence, Statistics & Probability Letters, 7, 283-286, https://doi.org/10.1016/0167-7152(89)90106-5, 1989.
Kabluchko, Z., Schlather, M., and de Haan, L.: Stationary Max-Stable Fields Associated to Negative Definite Functions, The Annals of Probability, 37, 2042-2065, 2009.
Kao, S.-C., and Govindaraju, R. S.: Trivariate statistical analysis of extreme rainfall events via the Plackett family of copulas, Water Resources Research, 44, doi:10.1029/2007WR006261, 2008.
Kleiber, W., Katz, R. W., and Rajagopalan, B.: Daily spatiotemporal precipitation simulation using latent and transformed Gaussian processes, Water Resources Research, 48, doi:10.1029/2011WR011105, 2012.
Koutsoyiannis, D., Kozonis, D., and Manetas, A.: A mathematical framework for studying rainfall intensity-duration-frequency relationships, Journal of Hydrology, 206, 118-135, http://dx.doi.org/10.1016/S0022-1694(98)00097-3, 1998.
Kuichling, E.: The relation between the rainfall and the discharge of sewers in populous districts, Transactions of the American Society of Civil Engineers, 20, 1-56, 1889.
Laurenson, E. M., and Mein, R. G.: RORB Version 4 Runoff Routing Program User Manual, Monash University Department of Civil Engineering, 1997.
Le, P. D., Davison, A. C., Engelke, S., Leonard, M., and Westra, S.: Dependence properties of spatial rainfall extremes and areal reduction factors, Journal of Hydrology, 565, 711-719, https://doi.org/10.1016/j.jhydrol.2018.08.061, 2018a.
Le, P. D., Leonard, M., and Westra, S.: Modeling Spatial Dependence of Rainfall Extremes Across Multiple Durations, Water Resources Research, 54, 2233-2248, doi:10.1002/2017WR022231, 2018b.
Ledford, A. W., and Tawn, J. A.: Statistics for Near Independence in Multivariate Extreme Values, Biometrika, 83, 169-187, 1996.
Leonard, M., Lambert, M. F., Metcalfe, A. V., and Cowpertwait, P. S. P.: A space-time Neyman–Scott rainfall model with defined storm extent, Water Resources Research, 44, doi:10.1029/2007WR006110, 2008.
Leonard, M., Westra, S., Phatak, A., Lambert, M., Hurk, B. v. d., McInnes, K., Risbey, J., Schuster, S., Jakob, D., and Stafford-Smith, M.: A compound event framework for understanding extreme impacts, Wiley Interdisciplinary Reviews: Climate Change, 5, 113-128, doi:10.1002/wcc.252, 2014.
Mulvaney, T. J.: On the use of self-registering rain and flood gauges in making observation of the relation of rainfall and floods discharges in a given catchment, Proc. Civ. Eng. Ireland, 4, 18–31, 1851.
Nicolet, G., Eckert, N., Morin, S., and Blanchet, J.: A multi-criteria leave-two-out cross-validation procedure for max-stable process selection, Spatial Statistics, 22, 107-128, https://doi.org/10.1016/j.spasta.2017.09.004, 2017.
Oesting, M., Schlather, M., and Friederichs, P.: Statistical post-processing of forecasts for extremes using bivariate Brown-Resnick processes with an application to wind gusts, Extremes, 20, 309-332, 10.1007/s10687-016-0277-x, 2017.

688 Opitz, T.: Extremal t processes: Elliptical domain of attraction and a spectral representation, Journal of
689 Multivariate Analysis, 122, 409-413, https://doi.org/10.1016/j.jmva.2013.08.008, 2013.
690 Padoan, S. A., Ribatet, M., and Sisson, S. A.: Likelihood-Based Inference for Max-Stable Processes,
691 Journal of the American Statistical Association, 105, 263-277, 10.1198/jasa.2009.tm08577, 2010.
692 Pathiraja, S., Westra, S., and Sharma, A.: Why continuous simulation? The role of antecedent moisture
693 in design flood estimation, Water Resources Research, 48, doi:10.1029/2011WR010997, 2012.
694 Pickands, J.: Statistical Inference Using Extreme Order Statistics, The Annals of Statistics, 3, 119-131,
695 10.2307/2958083, 1975.
696 Rahman, A., Weinmann, P. E., Hoang, T. M. T., and Laurenson, E. M.: Monte Carlo simulation of flood
697 frequency curves from rainfall, Journal of Hydrology, 256, 196-210, https://doi.org/10.1016/S0022-
698 1694(01)00533-9, 2002.
699 Rasmussen, P. F.: Multisite precipitation generation using a latent autoregressive model, Water
700 Resources Research, 49, 1845-1857, doi:10.1002/wrcr.20164, 2013.
701 Renard, B., and Lang, M.: Use of a Gaussian copula for multivariate extreme value analysis: Some case
702 studies in hydrology, Advances in Water Resources, 30, 897-912,
703 http://dx.doi.org/10.1016/j.advwatres.2006.08.001, 2007.
704 Requena, A. I., Chebana, F., and Ouarda, T. B. M. J.: A functional framework for flow-duration-curve
705 and daily streamflow estimation at ungauged sites, Advances in Water Resources, 113, 328-340,
706 https://doi.org/10.1016/j.advwatres.2018.01.019, 2018.
707 Russell, B. T., Cooley, D. S., Porter, W. C., and Heald, C. L.: Modeling the spatial behavior of the
708 meteorological drivers' effects on extreme ozone, Environmetrics, 27, 334-344, doi:10.1002/env.2406,
709 2016.
710 Schlather, M.: Models for Stationary Max-Stable Random Fields, Extremes, 5, 33-44,
711 10.1023/A:1020977924878, 2002.
712 Seneviratne, S. I., Nicholls, N., Easterling, D., Goodess, C. M., Kanae, S., Kossin, J., Luo, Y., Marengo,
713 J., McInnes, K., and Rahimi, M.: Managing the Risks of Extreme Events and Disasters to Advance
714 Climate Change Adaptation: Changes in Climate Extremes and their Impacts on the Natural Physical
715 Environment, 2012.
716 Nambucca Heads Flood Study:
717 http://www.nambucca.nsw.gov.au/cp_content/resources/16152_2011__Nambucca_Heads_Flood_Stu
718 dy_Final_Draft_Chapter_6a.pdf, 2011.
719 Stedinger, J., Vogel, R., and Foufoula-Georgiou, E.: Frequency Analysis of Extreme Events, in:
720 Handbook of Hydrology, edited by: Maidment, D. R., McGraw-Hill, New York, 18.11-18.66, 1993.
721 Stephenson, A. G., Lehmann, E. A., and Phatak, A.: A max-stable process model for rainfall extremes
722 at different accumulation durations, Weather and Climate Extremes, 13, 44-53,
723 https://doi.org/10.1016/j.wace.2016.07.002, 2016.
724 Thibaud, E., Mutzner, R., and Davison, A. C.: Threshold modeling of extreme spatial rainfall, Water
725 Resources Research, 49, 4633-4644, 10.1002/wrcr.20329, 2013.
726 Wadsworth, J. L., and Tawn, J. A.: Dependence modelling for spatial extremes, Biometrika, 99, 253-
727 272, 10.1093/biomet/asr080, 2012.
728 Wang, Q. J.: A Bayesian Joint Probability Approach for flood record augmentation, Water Resources
729 Research, 37, 1707-1712, 10.1029/2000WR900401, 2001.
730 Wang, Q. J., Robertson, D. E., and Chiew, F. H. S.: A Bayesian joint probability modeling approach
731 for seasonal forecasting of streamflows at multiple sites, Water Resources Research, 45,
732 doi:10.1029/2008WR007355, 2009.
733 Wang, X., Gebremichael, M., and Yan, J.: Weighted likelihood copula modeling of extreme rainfall
734 events in Connecticut, Journal of Hydrology, 390, 108-115,
735 http://dx.doi.org/10.1016/j.jhydrol.2010.06.039, 2010.
736 Westra, S., and Sisson, S. A.: Detection of non-stationarity in precipitation extremes using a max-stable
737 process model, Journal of Hydrology, 406, 119-128, http://dx.doi.org/10.1016/j.jhydrol.2011.06.014,
738 2011.
739 WMAWater: Review of Bellinger, Kalang and Nambucca River Catchments Hydrology, Bellingen
740 Shire Council, Nambucca Shire Council, New South Wales Government, 2011.

741 Zhang, L., and Singh, V. P.: Gumbel–Hougaard Copula for Trivariate Rainfall Frequency
742 Analysis, Journal of Hydrologic Engineering, 12, 409-419, doi:10.1061/(ASCE)1084-
743 0699(2007)12:4(409), 2007.
744 Zheng, F., Westra, S., and Leonard, M.: Opposing local precipitation extremes, Nature Clim. Change,
745 5, 389-390, 10.1038/nclimate2579

746 http://www.nature.com/nclimate/journal/v5/n5/abs/nclimate2579.html#supplementary-information,
747 2015.
748 Zscheischler, J., Westra, S., van den Hurk, B. J. J. M., Seneviratne, S. I., Ward, P. J., Pitman, A.,
749 AghaKouchak, A., Bresch, D. N., Leonard, M., Wahl, T., and Zhang, X.: Future climate risk from
750 compound events, Nature Climate Change, 8, 469-477, 10.1038/s41558-018-0156-3, 2018.

751